Materials Chemistry and Physics 146 (2014) 58–64

Contents lists available at ScienceDirect

Materials Chemistry and Physics

journal homepage: www.elsevier.com/locate/matchemphys

Ferrimagnetism and spin excitation in a Ni–Mn partially inverted spinel prepared using a modified polymeric precursor method

Rafael A. Ferreira [a,b], Julio C.G. Tedesco [c], Jonas O. Birk [c], Walter Kalceff [d,*], Fabiano Yokaichiya [e,f], Nina Rasmussen [c], Octavio Peña [b], Paul F. Henry [g], Giovanna G. Simeoni [h], Heloisa N. Bordallo [c,g], Paulo N. Lisboa-Filho [i]

[a] Programa de Pos-Graduação em Ciência e Tecnologia de Materiais (POSMAT), Universidade Estadual Paulista, Faculdade de Ciências, Caixa Postal 473, 17033-360 Bauru, São Paulo, Brazil
[b] Institut des Sciences Chimiques de Rennes – UMR 6226, Université de Rennes 1, F-35042 Rennes, France
[c] The Niels Bohr Institute, University of Copenhagen, DK-2100 Copenhagen, Denmark
[d] School of Physics and Advanced Materials, University of Technology Sydney (UTS), P.O. Box 123, Broadway, NSW 2007, Australia
[e] Laboratório Nacional de Luz Síncrotron (LNLS), Caixa Postal 6192, CEP 13083-970 Campinas, São Paulo, Brazil
[f] Comissao Nacional de Energia Nuclear (CNEN), Instituto de Pesquisas Energeticas e Nucleares (IPEN), Reactor Multiproposito Brasileiro (RMB), Avenida Lineo Prestes 2242, Bloco A, Cidade Universitaria Armando Salles de Oliveira, Sao Paulo, Brazil
[g] European Spallation Source ESS AB, Box 176, 22100 Lund, Sweden
[h] Heinz Maier-Leibnitz Zentrum (MLZ) and Physics Department, Technische Universität München, Lichtenbergstr. 1, 85748 Garching, Germany
[i] Universidade Estadual Paulista, Departamento de Física, Faculdade de Ciências, Caixa Postal 473, 17033-360 Bauru, São Paulo, Brazil

HIGHLIGHTS

- Ni–Mn oxide partially-inverted spinel made by modified polymeric precursor method.
- Magnetic measurements showed a ferrimagnetic and a parasitic magnetic transition.
- NPD revealed a magnetic structure consistent with a star-like moment arrangement.
- INS measurements indicated four distinct temperature-dependent magnetic regimes.

ARTICLE INFO

Article history:
Received 31 October 2013
Received in revised form
4 February 2014
Accepted 27 February 2014

Keywords:
Magnetic materials
Chemical synthesis
X-ray scattering
Neutron scattering and diffraction
Rietveld analysis
Magnetic structures

ABSTRACT

We demonstrate that a Ni–Mn oxide partially inverted spinel $(Ni_{1-\nu}Mn_{\nu})[Ni_{\nu}Mn_{2-\nu}]O_4$ having inversion degree $\nu \approx 0.8$ and produced by a modified polymeric precursor method exhibits behaviour previously reported only in monophased samples. The structure of the specimen was determined using Rietveld analysis of X-ray and neutron powder diffraction data, showing that at room temperature the material crystallizes in the $Fd\bar{3}m$ space group with a lattice constant $a = 8.392$ Å. Combining magnetization measurements with neutron powder diffraction, we show that the magnetic structure of this spinel is associated with the interplay between the ferromagnetic and antiferromagnetic lattices which coexist due to the cations' presence on both tetrahedral and octahedral sites. Our analysis of the neutron diffraction data confirms the postulated magnetic structure involving a star-like moment arrangement, arising from competition for the *B* (octahedral) spinel sites by the Ni and Mn cations. Finally, we show that strong magnetic fluctuations are observed in the inelastic neutron scattering data.

1. Introduction

Oxide spinels can exhibit a variety of magnetic moment configurations in the ground state, including collinear, canted and spiral ferromagnetic (FM), and antiferromagnetic (AFM) structures [1]. They are also known to be very attractive candidates for applications in spintronics [2], due to a large tunnelling magnetoresistance (TMR) response and high Curie temperatures (T_c) combining to produce either conductive or insulating behaviour. Indeed, the renewed interest in spinels with non-collinear magnetic structures is related to the multiferroic properties produced by the modulation of spiral spin configurations.

* Corresponding author.
E-mail addresses: wkalceff@uts.edu.au, wkalceff@gmail.com (W. Kalceff).

http://dx.doi.org/10.1016/j.matchemphys.2014.02.042
0254-0584/

The relation between the crystallographic and magnetic properties in advanced oxide spinel materials such as manganites is still not fully understood. It is interesting, therefore, to study such compounds in order to establish any eventual correlation which may lead to potential applications, as was the case, for instance, with the giant-magnetoresistance ferromagnetic perovskites [3] and in the application of mesoporous $NiMn_2O_x$ to electrochemical energy storage and catalytic decomposition [4].

Spinel-type structures occur in three common forms. The first has formula $(A)[B_2]O_4$, where the notation (A) denotes a tetrahedral site occupied by cation *A* and having four oxygens as nearest neighbours, while $[B_2]$ denotes an octahedral site occupied by two *B* cations with six oxygen atoms as nearest neighbours [5–8]. Using the same notation, the second structure—known as a *perfectly inverted spinel*—has formula $(B)[AB]O_4$. There is also an intermediate structural possibility, represented by $(A_{1-\nu}B_\nu)[A_\nu B_{1-\nu}]O_4$; here ν is the inversion degree, which can be affected by the atmosphere and heat treatment used in its preparation [9,10]. Generally, spinel systems crystallize as face-centred cubic (FCC) or body-centred tetragonal (BCT) structures in which the oxide anions (O^{2-}) occupy preferential positions, while the metallic cations (A^{2+} and B^{3+}) are distributed in tetrahedral and octahedral sites, respectively.

$NiMn_2O_4$ possesses a spinel-type structure with a certain degree of inversion and showing a rich magnetic response, including AFM, FM or ferrimagnetism, depending on the cation occupancy and oxygen content [10,11]. The complexity of the magnetic behaviour is related to the fact that Ni^{2+} and Mn^{3+} ($3d^4$) occupy octahedral sites, while Mn^{2+} ($3d^5$) and Mn^{4+} ($3d^3$) have a preference for tetrahedral sites. However, the ferri-paramagnetic transition temperature in this material is extremely dependent on the synthesis process. For instance, ferrimagnetic behaviour has been observed, with strong antiferromagnetic interactions producing large negative Curie–Weiss temperatures [5,7,12] and Curie temperatures varying from 100 K to 145 K [7,12–14]. Therefore, a controlled synthesis process opens the possibility for materials to be developed with desirable structural and micro-structural properties, and therefore may generate a better understanding of the magnetic behaviour of these systems.

Chemical methods for metallic oxide preparation have been used for several years as an excellent alternative to traditional solid-state reaction routes, the latter invariably producing unreactive, inhomogeneous samples with undesirable secondary phases and large grains. On the other hand, the modified polymeric precursor (MPP) method has been used reliably to produce high quality samples without these shortcomings [15]. The MPP method involves the polyesterification of a metal chelate complex using a hydroxycarboxylic acid and a polyhydroxy alcohol in an aqueous solution of metal ions to produce a polymeric gel. Subsequent heat treatment produces an amorphous powder which is then calcined to achieve a product of the desired unsegregated phase. This material is an extremely homogeneous, very fine, agglomerate-free ceramic powder which is reactive at temperatures significantly lower than those required for powders obtained by traditional routes [15].

Another point of interest in the study of $NiMn_2O_4$ is that it can present different physical behaviours depending on the size and shape of the final material. Bulk systems usually exhibit a ferrimagnetic to paramagnetic transition at about 100 K followed by a parasitic ferrimagnetic transition at lower temperatures, around 70 K [7], while nanoscale materials exhibit only one ferrimagnetic to paramagnetic transition around 105 K [8]. Interestingly, thin films seem to exhibit both behaviours, depending on the heat treatment [16].

In this paper we present results obtained from X-ray (XPD) and neutron powder diffraction (NPD) measurements on a ceramic oxide of nominal composition $NiMn_2O_4$, prepared using the MPP method. We show that the use of this method can improve the purity of the resulting material. Its magnetic behaviour was determined from magnetization measurements as functions of temperature (M–T) and applied magnetic field (M–H). By correlating the nuclear and magnetic structures obtained using Rietveld analysis to the bulk magnetic data, we were able to confirm a star-like magnetic configuration formed by the Mn and Ni moments in this compound. Furthermore, inelastic neutron scattering showed the presence of collective magnetic excitations below 40 K.

2. Experimental

The synthesis procedure used to obtain nickel manganate was the modified polymeric precursor (MPP) method [15], wherein stoichiometric amounts of the reagents $MnCO_3$, $Co(NO_3)_3 \cdot H_2O$ and Ni_2O_3 (all $\geq$ 99.9% purity) were weighed and mixed with nitric acid while stirring at a temperature of 70 °C. After visually checking for the formation of a metallic cation solution, a citric acid solution was added to the reagents to enhance the metallic cation chelation, and ethylene glycol was used to enhance the polyesterification of metallic citrate. The pH of the resulting solution was adjusted to a value of 3 by adding ethylenediamine. Stirring was maintained at a temperature of 70 °C until the elimination of volatiles and water was complete. The homogeneous polymer gel produced was then air-dried in a furnace at 350 °C for 4 h. The resulting powder was macerated in an agate mortar, heated at 800 °C for 4 h and finally heated at 1000 °C for 16 h.

The homogeneity of the sample was confirmed with energy dispersive X-ray (EDX) mapping in a Leo Stereoscan 440 scanning electron microscope (SEM). X-ray diffraction (XRD) analysis was performed with a Rigaku DMAX-2100/PC diffractometer using CuK_α (K_β-filtered) radiation (λ = 1.5406 Å). Room temperature 2θ scans from 10° to 100° in steps of 0.02° and at fixed counting times of 1.6 s were recorded. More detailed crystallographic studies were later performed at the Brazilian Synchrotron Light Laboratory (LNLS) on the X-ray powder diffraction beamline [17], with energies in the Fe-absorption K-edge (λ = 1.6650 Å) and Mn K-edge (λ = 1.5406 Å), using a six-circle Huber diffractometer and a step size of 0.02°. A germanium (111) crystal analyzer was used to achieve high resolution, the X-ray scans being measured in the 2θ range 15°–120°. Structural refinements were carried out by the Rietveld method [18,19] using GSAS [20], based on JCPDS phase identification data (2003) and the ICSD (2003) structural database. The sample diffraction profiles were modelled using the pseudo-Voigt Thompson–Cox–Hastings (TCH) function [21].

The magnetic structure was inferred from data taken on the high resolution neutron powder diffractometer E9 at the Berlin Neutron Scattering Center (BENSC) at the Helmholtz-Zentrum Berlin (HZB). The data were measured in zero magnetic field as a function of temperature between 2 K and 280 K at a wavelength of 1.797 Å, giving a resolution (full width at half maximum, FWHM) of $\Delta d/d \sim 0.2\%$. Neutron data were analysed by the Rietveld method using the FULLPROF suite of programs [22].

Bulk magnetization measurements were performed using a Quantum Design 6000 magnetometer with both zero field cooling (ZFC) and field cooling (FC) between 10 K and 300 K using applied fields of 100 Oe, 500 Oe and 1 kOe. Magnetic hysteresis curves were measured between 10 K and 300 K in a field range of −9 kOe to +9 kOe. These measurements allowed the evolution of the magnetic properties of the material to be followed.

Finally, inelastic neutron scattering (INS) measurements were performed using the TOFTOF spectrometer [23] at the Garching research reactor (FRM-II), Munich. A wavelength of 5 Å and a chopper velocity of 16,000 rpm were selected as a compromise

between a good elastic resolution of 100 μeV (FWHM), large enough q-range (2.2 $Å^{-1}$) and sufficient intensity. The sample was placed in a cylindrical aluminium can and data were recorded at a range of temperatures from 4 K to 110 K. The raw data were processed by subtracting the scattering from an empty can and normalizing to a vanadium scan. Standard data treatments were performed using MATLAB procedures.

3. Results and discussion

SEM-EDX analysis of the $NiMn_2O_4$ sample prepared using the MPP method showed the expected stoichiometric ratios of the constituent elements. Fig. 1 is an SEM image of the specimen, with a distribution of particle diameters ranging from sub-micron to several microns. Mapping of the elements Ni, Mn and O using EDX showed a uniform distribution throughout the material, with no agglomeration. Moreover, Rietveld refinement of the $NiMn_2O_4$ XPD data at room temperature for a sample treated at 1000 °C for 16 h gave a lattice constant $a = 8.392$ Å, in agreement with values obtained from specimens prepared by other methods [7,8,24].

In crystalline spinel-type structures such as the system here, the metallic cations occupying the tetrahedral sites are often divalent (in our case, Ni^{2+} and Mn^{2+}), while the trivalent cations occupy both sites (Mn^{3+} in our sample). In $NiMn_2O_4$ it is expected that the Ni^{2+} ($3d^8$), Mn^{3+} ($3d^4$) and Mn^{4+} ($3d^3$) cations will preferentially occupy the octahedral sites, while the Mn^{2+} ($3d^5$) cations will occupy the tetrahedral ones [25]. A common approach to accurately resolving such site occupancy questions is to use X-ray anomalous diffraction to analyse the charge balance. Such analyses also provide a means of verifying the oxidation states of the manganese, which in $NiMn_2O_4$ are expected to be (III) and (IV). To resolve this question, we used program FPRIME [26] to estimate the scattering factors in the absorption K edge of Fe (1.6500 Å) and Mn (1.8962 Å). As seen in Table 1, we obtained different anomalous scattering for Ni, Mn and O in the whole 2θ range, thus confirming the occupancy factors for the tetragonal and octahedral sites in these spinel structures.

As a second step in the characterization of our bulk samples using the XPD data, we were able to determine the oxygen positions, the atomic displacements (UISO) and the occupancy factors of Mn and Ni. The final refined values are given in Table 1. Interestingly, we note that while in normal spinels the divalent cations (e.g. Ni^{2+}) preferentially occupy the tetrahedral (A) sites and the trivalent cations (e.g. Mn^{3+}) occupy the octahedral (B) sites, the refined data of Table 1 shows them to be distributed on both crystallographic sites. It can therefore be concluded that the spinel undergoes an inversion transformation, thus confirming the expected results of crystal field stabilization energy (CFSE) calculations [27]. Therefore, the composition of this particular synthesized spinel can be written as $(Ni_{0.20}Mn_{0.80})_{tet}[Ni_{0.84}Mn_{1.16}]_{oct}O_4$.

Table 1
Summary of results from the Rietveld analysis of XPD data for MPP-prepared nickel manganite sample at room temperature and at two wavelengths. The space group used was $Fd\bar{3}m$, and the Ni and Mn atoms were considered to occupy both tetrahedral (0.125,0.125,0.125) and octahedral (0.5,0.5,0.5) sites.

	f'	f''
$\lambda = 1.6500$ Å		
Ni	−1.964	0.586
Mn	−1.084	3.17
O	0.056	0.038
$\lambda = 1.8962$ Å		
Ni	−1.354	0.739
Mn	−9.009	0.462
O	0.069	0.050

Atoms	x	y	z	Occupancy	UISO
O	0.2624	0.2624	0.2624	1	0.028296
Mn(tet.)	0.125	0.125	0.125	0.80	0.011351
Ni(tet.)	0.125	0.125	0.125	0.20	0.011351
Mn(oct.)	0.5	0.5	0.5	0.58	0.004206
Ni(oct.)	0.5	0.5	0.5	0.42	0.004206

We now turn to the magnetic properties of our specimen, elucidated via volumetric magnetization measurements. Fig. 2 shows the magnetization as a function of temperature measured in ZFC and FC cycles in an applied magnetic field $H = 100$ Oe. The observed irreversibility at $T_{irr} = 91$ K between the ZFC and FC curves is a well-known characteristic of ferrimagnetic materials [28,29]. This thermal hysteresis is usually observed in spinel-type systems in which different crystallographic sites are occupied by the same cation, consistent with our Rietveld refinements. The inset of Fig. 2 shows the derivative of the FC curve, indicating the ferrimagnetic transition T_c at 96 K together with changes in the magnetic configuration of the system at $T_m = 105$ K, $T_1 = 77$ K and at $T_2 = 63$ K. T_m is the setting point of the ferri-paramagnetic transition, while T_1 and T_2 are related to parasitic magnetic transitions [5] occurring before the ferrimagnetic–paramagnetic transition at T_c, attributed to a transition from a Yafet–Kittel (triangular) configuration to a collinear Néel state. Later in our paper this behaviour

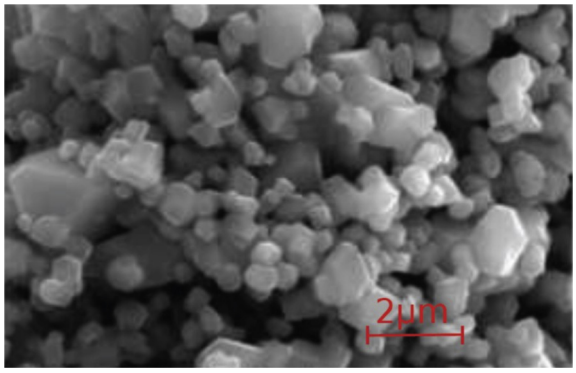

Fig. 1. Scanning electron micrograph of a representative sample of nickel manganite powder obtained by the modified polymeric precursor method, followed by heat treatment in air at 1000 °C for 16 h.

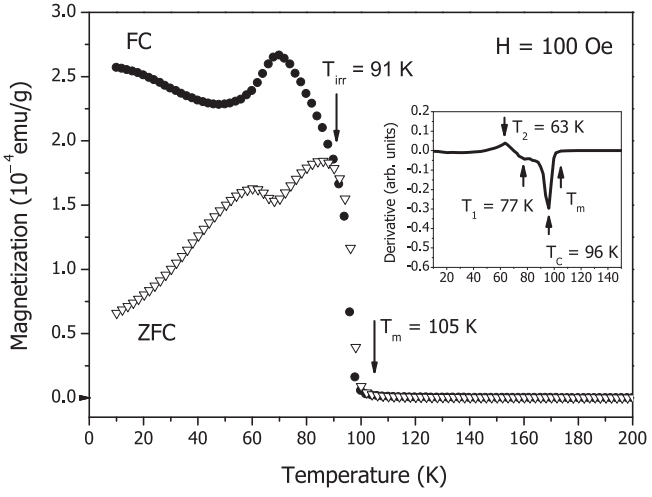

Fig. 2. Magnetization versus temperature plots for $(Ni_{0.20}Mn_{0.80})_{tet}[Ni_{0.84}Mn_{1.16}]_{oct}O_4$ at a constant applied field of 100 Oe. The closed circles denote the FC curve and the open triangles the ZFC curve. The inset figure shows the derivate of the FC data, with the magnetic transition temperatures indicated.

will be related to the configuration of the magnetic structure. The observed T_m and T_c are similar to those previously reported in the literature [5,7–9,12].

As shown in Fig. 3(a) and (b), increasing the applied magnetic field causes an enhancement in the measured magnetization and a clear reduction of T_{irr}, while T_c remains constant. The shape of the magnetisation curves indicates a ferrimagnetic ordering caused by the interplay between the sublattices, with both cooperative (FM) and competitive (AFM) mechanisms being present. Considering the Curie–Weiss model, the predominant magnetic interaction can be determined by extrapolating the inverse magnetic susceptibility–temperature curve ($1/\chi$ vs T) in the paramagnetic state, as shown in the inset of Fig. 3(b). A negative Curie–Weiss temperature $\theta = -78$ K and an effective magnetic moment of $\mu_{eff} = 5.89$ μB are obtained and are similar to previously reported values [12]; thus, we can conclude that the AFM interactions are predominant in this system.

To further verify our assumptions about the magnetic structure of the sample, NPD studies were carried out. In the NPD data refinement the same cubic spinel structure as determined from the X-ray data was used at all temperatures, with Mn (80%) and Ni (20%) at tetrahedral Wyckoff positions 8a (0.125,0.125,0.125) and Mn (58%) and Ni (42%) at octahedral Wyckoff positions 16d (0.5,0.5,0.5). The O atoms are located on Wyckoff positions 32e (x,x,x) with $x = 0.2624(8)$. The atom positions were taken from Boucher et al. [12]. Magnetic scattering was observed below 100 K and was simultaneously refined with the nuclear scattering contribution, as shown in Fig. 4. It should be noted that until now Ni–Mn spinels had been obtained by different routes to ours [7,8]. For instance, a study by Almeida et al. [8] showed that the $NiMn_2O_4$

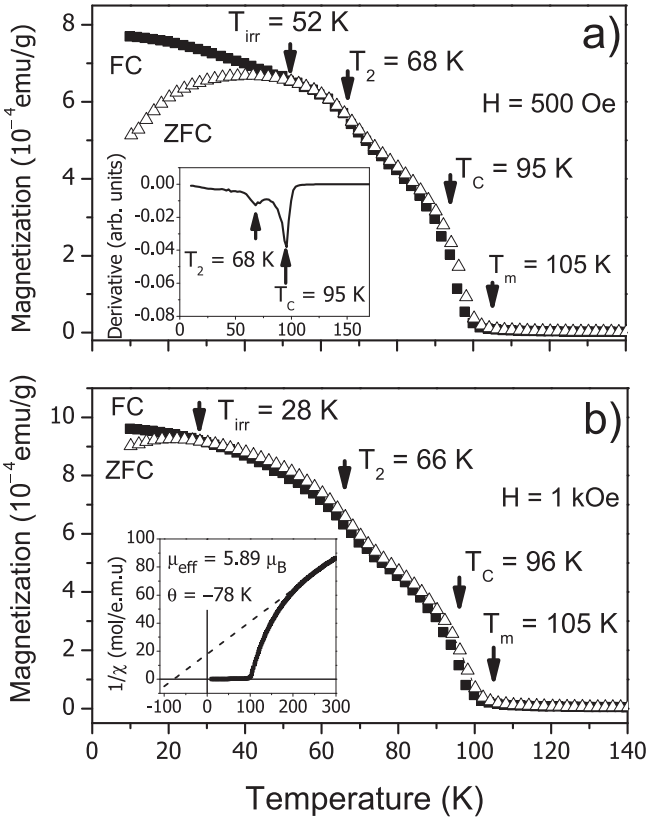

Fig. 3. (a) and (b) (main plots) Magnetization Vs temperature at constant applied fields of 500 Oe and 1 kOe, respectively; inset (a) derivative of magnetisation versus temperature; inset (b) inverse susceptibility versus temperature.

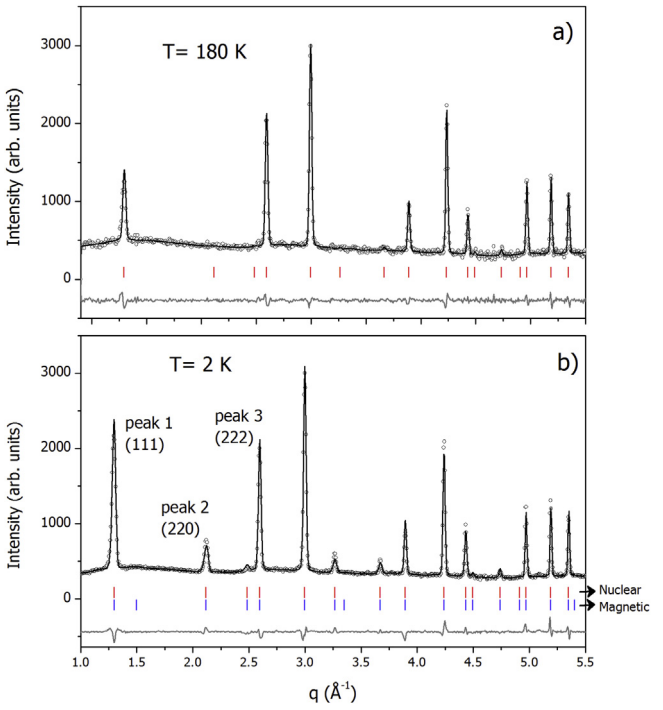

Fig. 4. Rietveld refinement of NPD data for sample $(Ni_{0.20}Mn_{0.80})_{tet}[Ni_{0.84}Mn_{1.16}]_{oct}O_4$ measured on E9–BERII–HZB at (a) 180 K and (b) 2 K in zero field using $\lambda = 1.797$ Å. The circles represent the experimental data, while the black and grey lines correspond (respectively) to the refined intensities and the difference plot between the calculated and observed intensities. The top row of vertical (red) marks on both plots show the calculated positions of the Bragg reflections in $NiMn_2O_4$. The bottom row of (blue) marks in (b) indicates the calculated positions of the magnetic reflections. (For interpretation of the references to colour in this figure legend, the reader is referred to the web version of this article.)

obtained from xerogels in a process similar to the MPP method produced nanoparticles when allowed to crystalise at 600 °C; however, a high content of secondary phases was present. Díez et al. [7] reported the synthesis of the same material through thermal decomposition yielding 3% impurities, while Sagua et al. [24] (using a hydroxide route) obtained a slightly Ni-defective global stoichiometry, attributed to the presence of 1.6(1)% NiO. Within the accuracy of the data, no evidence of impurity phases was observed in our method.

Structural parameters determined by the Rietveld analysis of the NPD data are shown as a function of temperature in Fig. 5. A spherical harmonics approach was used to model the scattering contributions in the Rietveld refinement, considering the Mn atoms in a primitive unit cell at the *A* sites, and Mn and Ni atoms at the *B* sites, as reported previously [9,12,14,28,29]. Our analysis confirmed that the magnetic structure consists of a star-like arrangement of moments, as shown schematically in Fig. 6. This model is effectively a three-sublattice model, first described by Boucher et al. [29] in 1970, where the magnetic moments of sublattice *A* interact differently with the magnetic moments of sublattice *B*, depending on the magnetic ion that occupies the site *B* (Mn or Ni). This is also in agreement with the previously mentioned Yafet–Kittel configuration. It is seen from Fig. 5(a) that the cubic lattice constant *a*, as well as the Mn–Ni bond lengths (i.e. distances between the *A* and *B* sites) vary approximately linearly with temperature between 50 K and 280 K. The Mn–Mn bond lengths (i.e. distances between the *B* sites) vary as shown in Fig. 5(b), having a similar linear thermal expansion behaviour over this temperature range. On the other hand, the Mn–O bond lengths plotted in Fig. 5(b) remain

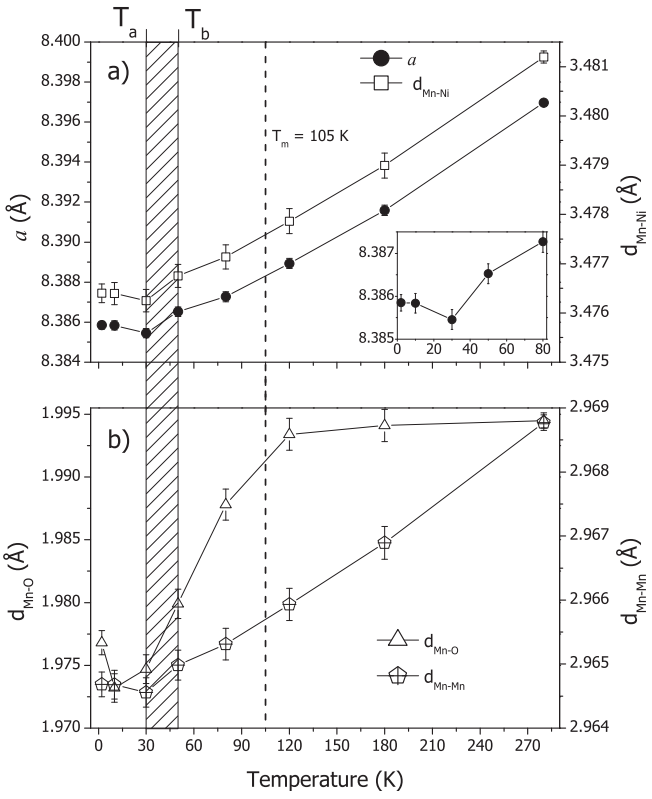

Fig. 5. (a) Temperature dependence of the lattice constant a and the Mn–Ni bond length (distance between the A and B sites); (b) Mn–Mn bond lengths (distance between the B sites) and Mn–O bond lengths as a function of temperature. The dashed line is a visual guide for comparison of the two plots. T_m indicates a ferrimagnetic transition, when the magnetic peaks start to appear. Also, a magnetostriction is observed at a temperature within a range indicated by the hatched region $T_a < T < T_b$ (with $T_a = 30$ K and $T_b = 50$ K) and is related to a second magnetic rearrangement of the lattice.

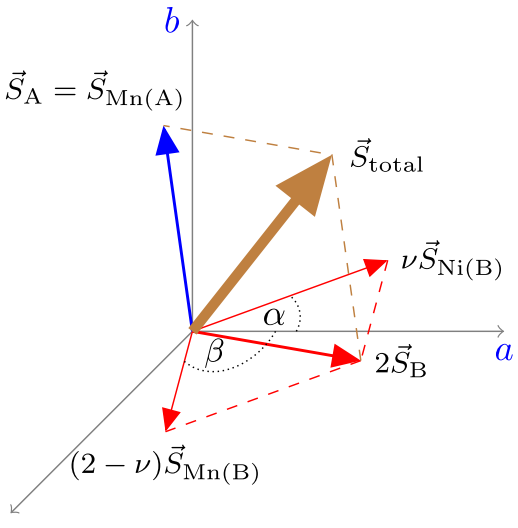

Fig. 6. Schematic representation of the star-like magnetic structure of $(Ni_{0.20}Mn_{0.80})_{tet}[Ni_{0.84}Mn_{1.16}]_{oct}O_4$. The blue arrow shows $\vec{S}_{Mn(A)}$, the magnetic moment of sublattice A, and the red arrows show $\nu\vec{S}_{Ni(B)}$, the magnetic moment for the Ni atom in the B sublattice, $(2-\nu)\vec{S}_{Mn(B)}$, the magnetic moment for the Mn atom in the B sublattice, and $2\vec{S}_B$, the resultant magnetic moment for the B sublattice. In the present case, $\nu \approx 0.8$, $\alpha \approx 60°$ and $\beta \approx 70°$. (For interpretation of the references to colour in this figure legend, the reader is referred to the web version of this article.)

temperature-invariant on cooling from 280 K (not shown) to 120 K and then decrease. The re-arrangement of the magnetic structure causes a small magnetostriction to be observed at lower temperatures, but the precise temperature of the onset of this behaviour cannot be specified due to the small number of available experimental points; hence it is shown in Fig. 5 as a hatched region between 30 K and 50 K.

Fig. 7(a) shows the integrated intensity around $\omega = 0$ extracted from the TOFTOF data at 4 K, together with the identification of the diffraction peaks. Peaks 1 and 2 are the (111) and (220) reflections already observed in the NPD data as shown in Fig. 4, while the broad hump identified as peak A is related to the magnetic fluctuations also seen in Fig. 4 and reported by Boucher et al. [12]. To better understand these features, the integrated intensities of peaks 1, 2 and 3 (the latter related to the (222) nuclear reflection) obtained from the analysis of the NPD data, are shown in Fig. 7(b). As the integrated intensities of peaks 1, 2 and 3 closely follow the evolution of the magnetization Vs temperature curve (see Fig. 3), they can be directly related to the magnetic ordering of the system. Of more interest, however, is the change in the behaviour of peak 3 occurring over the same (hatched) temperature range defined in Fig. 5. In Fig. 7(b), a very slight increase of the integrated intensity is observed, being more evident close to 50 K (T_b); a decrease in intensity occurs below 30 K (T_a). This behaviour closely follows the evolution of the lattice parameters and bond lengths shown in Fig. 5. Our observations appear to indicate a further rearrangement of the magnetic moments, and this idea is also supported by the inelastic neutron scattering results discussed below.

We now turn to the analysis of the INS data. Fig. 7(c) shows the scattering intensity with an energy transfer up to 8 meV as a function of temperature. In this region no phonon contribution is expected, therefore the observed fluctuations are attributed to magnetic scattering. Four temperature regimes can be identified:

i. $T > T_m$ (purple line (in the web version)) where the magnetic correlations have collapsed.
ii. $T_b < T < T_m$ (blue line) where due to the collinear arrangement of the moments the magnetic response becomes a broad inelastic contribution at 2 meV with a full width at half maximum of about 1 meV.
iii. $T_a < T < T_b$ (red line) where a significant broadening of the inelastic magnetic scattering intensities occurs, while the quasi-elastic signal, $\omega = 0$, seems to be unchanged. This behaviour is characteristic of a canted spin system, where due to the distribution of the magnetic moments among the different sites some type of a dynamical spin-frustration effect can be observed [30].
iv. $T < T_a$ (black line) where the inelastic intensity of $(Ni_{0.20}Mn_{0.80})_{tet}[Ni_{0.84}Mn_{1.16}]_{oct}O_4$ again reveals features of collective magnetic excitations around 3 meV. This response is similar to the excitation observed in (ii). This observation, together with the increase in intensity at energy equal to zero, seems to corroborate the idea that a new rearrangement of the spins occurs below T_a.

4. Conclusion

The Ni–Mn specimen obtained by a modified polymeric precursor method brings new insights into its magnetic properties, observed via magnetization, XPD, NPD and INS measurements. It is interesting to note that the data in Table 1 and other results obtained in this paper, when compared with the literature [7,8] support the conclusion that the MPP method yields monophased

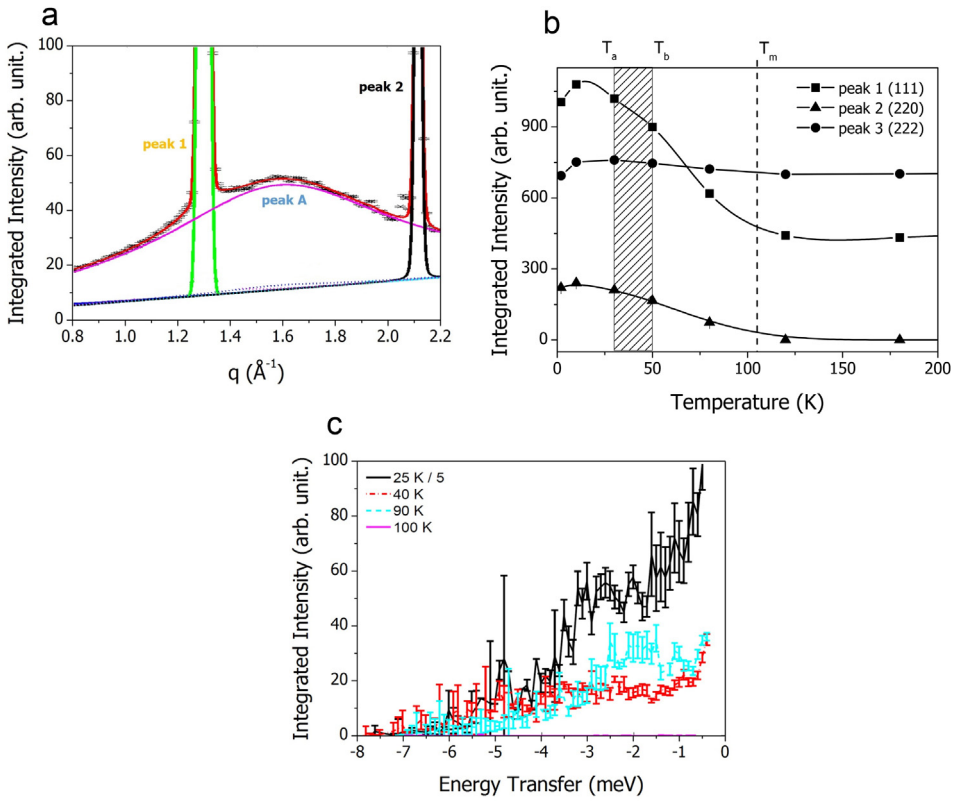

Fig. 7. (a) Peak intensities around $\omega = 0$, extracted from the TOFTOF data at 4 K, together with the identification of the diffraction peaks. (b) Temperature dependence of the integrated intensity of selected diffraction peaks observed in the E9 and TOFTOF data. (c) Dynamic structure factor of $(Ni_{0.20}Mn_{0.80})_{tet}[Ni_{0.84}Mn_{1.16}]_{oct}O_4$ at various temperatures.

samples. The high-temperature treatment causes an increase in crystallite size [8], as well as the formation of monophased material, which are essential to avoid contamination of the magnetic data.

Structural refinement using the Rietveld method showed that the specimen obtained is a bulk-like monophased material with a partially inverted spinel-type structure. The XPD data collected at two distinct wavelengths allowed the site occupancies of the structure to be refined, showing that it had an inversion parameter $\nu = 0.80$ and hence a nominal formula $(Ni_{0.20}Mn_{0.80})_{tet}[Ni_{0.84}Mn_{1.16}]_{oct}O_4$. ZFC and FC measurements showed typical behaviour for a ferrimagnetic material. The ensemble of ZFC–FC curves obtained at lower fields indicates a clear competition between two sublattices, AFM and FM, with a T_c and T_m close to 100 K. NPD data showed magnetic peaks appearing below 100 K, and the Rietveld refinement was consistent with the star-like magnetic structure reported by Boucher et al. [12], arising from the coexistence of Ni and Mn atoms in the *B* sites of the spinel structure. Of most interest was the observation of a collective magnetic excitation at very low temperatures which seems to be related to the observation of a small magnetostriction of the lattice.

Acknowledgements

The research of JCGT was supported by the *Brazilian Science Without Borders* program (funds from CNPq). RAF was financed by the bilateral exchange program France–Brazil CAPES–COFECUB, project number 706/11 through the Joint PhD International Program, UNESP-Université de Rennes 1. The work performed by JOB, NR and HNB was financed by Danscatt. WK acknowledges a travel grant from UTS allowing him to visit NBI while on sabbatical leave. All authors gratefully acknowledge BER2 and FRM2 for the provision of beam time.

References

[1] T. Rudolf, C. Kant, F. Mayr, J. Hemberger, V. Tsurkan, A. Loidl, Spin-phonon coupling in antiferromagnetic chromium spinels, New J. Phys. 9 (3) (2007) 76.
[2] U. Lüders, A. Barthélémy, M. Bibes, K. Bouzehouane, S. Fusil, E. Jacquet, J.-P. Contour, J.-F. Bobo, J. Fontcuberta, A. Fert, $NiFe_2O_4$: a versatile spinel material brings new opportunities for spintronics, Adv. Mater. 18 (13) (2006) 1733–1736.
[3] P.R. Savage, Giant Magnetoresistance: Technology and Markets for Sensors, Disk Storage, Mram, and Spintronics, John Wiley & Sons, Inc., 2000.
[4] Y. Ren, Z. Ma, P.G. Bruce, Ordered mesoporous $NiMn_2O_x$ with hematite or spinel structure: synthesis and application in electrochemical energy storage and catalytic conversion of N_2O, CrystEngComm 13 (23) (2011) 6955–6959.
[5] S. Åsbrink, A. Waśkowska, M. Drozd, E. Talik, Physical properties and X-ray diffraction of a $NiMn_2O_4$ single crystal below and above the ferrimagnetic transition at $T_c = 145$ K, J. Phys. Chem. Solids 58 (5) (1997) 725–729.
[6] H.T. Zhang, X.H. Chen, Size-dependent X-ray photoelectron spectroscopy and complex magnetic properties of $CoMn_2O_4$ spinel nanocrystals, Nanotechnology 17 (5) (2006) 1384.
[7] A. Díez, R. Schmidt, A.E. Sagua, M.A. Frechero, E. Matesanz, C. Leon, E. Morán, Structure and physical properties of nickel manganite $NiMn_2O_4$ obtained from nickel permanganate precursor, J. Eur. Ceram. Soc. 30 (12) (2010) 2617–2624.
[8] J. Almeida, C. Meneses, A. de Menezes, R. Jardim, J. Sasaki, Synthesis and characterization of $NiMn_2O_4$ nanoparticles using gelatin as organic precursor, J. Magn. Magn. Mater. 320 (14) (2008) e304–e307.
[9] P. Lisboa-Filho, M. Bahout, P. Barahona, C. Moure, O. Peña, Oxygen stoichiometry effects in spinel-type $NiMn_2O_{4-\delta}$ samples, J. Phys. Chem. Solids 66 (7) (2005) 1206–1212.
[10] K.P. Chae, J.-G. Lee, H.S. Kweon, Y.B. Lee, The crystallographic, magnetic properties of al, ti doped $CoFe_2O_4$ powders grown by sol–gel method, J. Magn. Magn. Mater. 283 (1) (2004) 103–108.
[11] Y. Shen, T. Nakayama, M. Arai, O. Yanagisawa, M. Izumi, Magnetic phase transition and physical properties of spinel-type nickel manganese oxide, J. Phys. Chem. Solids 63 (6–8) (2002) 947–950.
[12] B. Boucher, R. Buhl, M. Perrin, Etude cristallographique du manganite spinelle cubique $NiMn_2O_4$ par diffraction de neutrons, Acta Crystallogr. Sect. B Struct. Crystallogr. Cryst. Chem. 25 (11) (1969) 2326–2333.

[13] C. Boudaya, L. Laroussp, E. Dhahrp, J.C. Joubert, A. Cheikh-Rouhou, Preparation and characterization of the spinel series $Co_{6+x}Ni_{4-x}Mn_8O_{24}$ ($0 \leq x \leq 4$), Phase Trans. 68 (4) (1999) 631–642.
[14] O. Peña, X. Cailleaux, B. Piriou, M. del Canto, S. Abarca, E. Ríos, J. Ortiz, J. Gautier, P. Lisboa-Filho, C. Moure, Magnetic properties of $Cu_{1+x}Mn_{2-x}O_4$ and $Ni_{1+x}Mn_{2-x}O_4$ solid solutions, J. Eur. Ceram. Soc. 27 (13) (2007) 3911–3914.
[15] P. Lisboa-Filho, A. Mombru, H. Pardo, W. Ortiz, E. Leite, Influence of processing conditions on the crystal structure and magnetic behavior of $La_{0.7}Ca_{0.3}MnO_{3\pm\delta}$ samples, J. Phys. Chem. Solids 64 (4) (2003) 583–591.
[16] B. Nelson-Cheeseman, R. Chopdekar, J. Iwata, M. Toney, E. Arenholz, Y. Suzuki, Modified magnetic ground state in $NiMn_2O_4$ thin films, Phys. Rev. B 82 (14) (2010) 144419.
[17] F.F. Ferreira, E. Granado, W. Carvalho Jr., S.W. Kycia, D. Bruno, R. Droppa Jr., X-ray powder diffraction beamline at D10B of LNLS: application to the Ba_2FeReO_6 double perovskite, J. Synchrotron Radiat. 13 (1) (2005) 46–53.
[18] H. Rietveld, A profile refinement method for nuclear and magnetic structures, J. Appl. Crystallogr. 2 (2) (1969) 65–71.
[19] H. Rietveld, Line profiles of neutron powder-diffraction peaks for structure refinement, Acta Crystallogr. 22 (1) (1967) 151–152.
[20] A. Larson, R. Von Dreele, General Structure Analysis System (GSAS), Report LAUR 86-748, Los Alamos National Laboratory.
[21] P. Thompson, D. Cox, J. Hastings, Rietveld refinement of Debye–Scherrer synchrotron X-ray data from Al_2O_3, J. Appl. Crystallogr. 20 (2) (1987) 79–83.
[22] J. Rodríguez-Carvajal, Recent advances in magnetic structure determination by neutron powder diffraction, Phys. B Condens. Matter 192 (1) (1993) 55–69.
[23] T. Unruh, J. Neuhaus, W. Petry, The high-resolution time-of-flight spectrometer TOFTOF, Nucl. Instrum. Methods Phys. Res. Sect. A Accel. Spectrom. Detect. Assoc. Equip. 580 (3) (2007) 1414–1422.
[24] A. Sagua, G.M. Lescano, J. Alonso, R. Martínez-Coronado, M. Fernández-Díaz, E. Morán, Neutron structural characterization, inversion degree and transport properties of $NiMn_2O_4$ spinel prepared by the hydroxide route, Mater. Res. Bull. 47 (6) (2012) 1335–1338.
[25] D.F. Shriver, P.W. Atkins, Inorganic Chemistry, third ed., Oxford University Press, Oxford, 1999.
[26] R.B. von Dreele, FPrime for Windows, 1994 (cited 0ctober 2013), URL: http://www.ccp14.ac.uk/ccp/ccp14/ftp-mirror/gsas/public/gsas/windows/fprime.zip.
[27] K. Yatsimirskii, N. Kostromina, Crystal field stabilization energy in halides of the rare earth elements taking account of spin-orbital interaction, Theor. Exp. Chem. 2 (5) (1966) 436–439.
[28] B. Boucher, R. Buhl, M. Perrin, Structure magnetique a trois sous-reseaux dans l'approximation du champ moleculaire, J. Phys. Chem. Solids 30 (10) (1969) 2467–2477.
[29] B. Boucher, R. Buhl, M. Perrin, Structures magnetiques anisotropes dans les spinelles, J. Phys. Chem. Solids 31 (10) (1970) 2251–2266.
[30] K. Tomiyasu, H. Hiraka, K. Ohoyama, K. Yamada, Resonance-like magnetic excitations in spinel ferrimagnets $FeCr_2O_4$ and $NiCr_2O_4$ observed by neutron scattering, J. Phys. Soc. Jpn. 77 (12) (2008) 124703.